The Aeronautical Journal (2024), **128**, pp. 1429–1449
doi:10.1017/aer.2024.49

RESEARCH ARTICLE

Combustion characteristics of sustainable aviation fuels in a scaled-down afterburner test rig

J. Bae[1], S. Chaudhuri[1], P. Canteenwalla[2] and S. Yun[2]

[1]Institute for Aerospace Studies, University of Toronto, Toronto, ON, Canada
[2]National Research Council, Ottawa, ON, Canada
Corresponding author: S. Yun; Email: Sean.Yun@nrc-cnrc.gc.ca

Received: 27 October 2023; **Revised:** 4 April 2024; **Accepted:** 17 April 2024

Keywords: sustainable aviation fuel (SAF); in-tandem combustor; flame stability

Abstract

This study investigates the combustion characteristics (lean blowoff (LBO), flashback, and combustion instability) of sustainable aviation fuels (SAFs) using a two-staged combustor arranged in tandem. The combustor consists of a first (main) burner with an axial swirler and a second burner (afterburner) with a V-gutter bluff-body. The main burner utilises a constant flow rate of CH_4/Air as reactants, while the afterburner operates on the combustion product from the first burner, additional dilution air, and one of the six liquid test fuels (Jet-A, A-2, C-1, C-5, C-9, and JP-8/HRJ) as reactants. When test fuels with higher derived cetane number (DCN) are used in the afterburner, it is observed that LBO occurs at lower afterburner global equivalence ratios (ϕ_{af}). This is due to the smaller chemical time scale of those test fuels, which enables the flame to be sustained under higher flow speeds. This is consistent with the results of previous studies. Additionally, this study shows that flashback also occurs at lower equivalence ratio for test fuels with higher DCN. This is a new finding and can be explained in a similar way to LBO. As the operating conditions approach the LBO or exceed flashback limits, the reactivity of shear layer also decreases, creating favourable conditions for them to occur. Moreover, for test fuels with low DCN (C-1 and C-5), blowoff occurs instead of flashback as ϕ_{af} increases. This can be attributed to the stronger pressure perturbation resulting from combustion instability in these flames compared to others. It demonstrates a stronger correlation between the pressure perturbation and the heat release rate fluctuation for C-1 and C-5 than that of other test fuels at the same equivalence ratio. In conclusion, it was found that test fuels with higher DCN have advantages in terms of LBO and stability, however, they are more prone to flashback.

Nomenclature

CN	cetane number
CL	chemiluminescence
DCN	derived cetane number
DP	dynamic pressure sensor
DSLR	digital single-lens reflex
FOV	field of view
HOC	heat of combustion
HRJ	hydrotreated renewable jet
IQT	ignition quality test
LBO	lean blowoff
MFC	mass flow controller
MW	molecular weight

A version of this paper first appeared at the 26th Conference of the International Society for Air Breathing (ISABE), 22–27 September 2024, Toulouse, France.

NJFCP	national jet fuels combustion program
pdf	probability density function
PM	particulate matter
PMT	photomultiplier tube
RMS	root-mean-square
SAF	sustainable aviation fuels
SCR	sooty flame concentration ratio
TC	thermocouples

Symbols

Da	Damköhler number
I	relative reactivity in the shear layer compared to the average total flame
P	pressure
p'	pressure perturbation
q'	heat release rate fluctuation
T	temperature
t	time
t_p	period of oscillation
$\mathbf{X}$	phase space vectors
$\theta_{p'_3-q'}$	phase difference between the pressure perturbation near the V-gutter (p'_3) and the heat release rate fluctuation (q')
τ	time lag
τ_c	chemical time scale
τ_H	time constant for high-temperature chemistry
τ_i	ignition delay time
τ_L	time constant for low-temperature chemistry
τ_M	time constant for moderate-temperature chemistry
τ_r	residence time scale
ϕ_{af}	global equivalence ratio at the afterburner

1.0 Introduction

The operation of airlines has been significantly affected by the considerable price fluctuations of jet fuel and the enforcement of stricter emission regulations in response to climate change. Consequently, in order to ensure a stable supply of jet fuel, reduce the impact of oil price volatility, and tackle environmental issues, sustainable aviation fuels (SAFs) are currently under development [1, 2]. The drop-in ready feature, which allows the SAFs to be used without modifications to engines, aircraft components, or infrastructure, requires extensive testing, leading to significant costs and certification time [2]. The US-led National Jet Fuels Combustion Program (NJFCP) aimed to minimise and streamline this extensive testing procedure, focusing exclusively on the combustion operability aspects of these fuels, specifically lean blowoff (LBO) and ignition under cold start and altitude relight conditions [2]. In other words, it is important to understand the relationship between the properties of SAFs and their combustion characteristics to safely replace existing aviation fuels.

Previous studies using the SAFs have been identifying the characteristics of exhaust emissions [3], lean blowoff [4], ignition characteristics [5, 6], etc. Zheng et al. [7] analysed the effects of the characteristics of NJFCP test fuels on the particulate matter (PM) number, LBO, and sooty flame concentration ratio (SCR), and showed that derived cetane number (DCN), aromatic content, and hydrogen content are the dominant factors for the LBO, PM number, and SCR, respectively.

Most of the studies [8–10] on the LBO characteristics of SAFs showed a strong correlation between DCN and LBO. The cetane number (CN) indicates the ignition quality [11], where fuels with higher values of CN ignite more readily than fuels with lower CN values [12]. The cetane number of fuel blends can be characterised using DCN [13]. In simpler terms, a higher DCN indicates faster ignition and increases auto-ignition reactivity [13]. Blowoff represents the phenomenon that the flame cannot

https://doi.org/10.1017/aer.2024.49 Published online by Cambridge University Press

be stabilised in high velocity reactant streams [14]. LBO has been a big problem since the gas turbine was used as the propulsion system of aircraft and power plant. Won et al. [15] explored the changes in the LBO according to the air inlet temperature. They [15] showed that the DCN values of initial 20% distillation cuts and the chemical properties of the entire fuel sample are the most relevant to the LBO under the low air inlet temperature and under the high air inlet temperature, respectively.

In contrast to previous studies that focused on the characteristics of SAF using a single combustor, this research introduces a novel approach by designing and fabricating a two-staged combustor. The objective of NJFCP is to assess the applicability of alternative jet fuels for commercial and military uses [16]. Still, previous studies primarily assessed the applicability of SAF in civil aircraft, and did not focus on military-specific aircraft, such as afterburning engines. Consequently, understanding the flame characteristics of SAF in the afterburner becomes crucial. The afterburner is an additional engine component extensively employed in military aircraft engines, intended to augment aircraft thrust, particularly during supersonic and hypersonic flights, take-off, and combat scenarios [17]. The afterburner is composed of an extended exhaust section with additional fuel injectors. The afterburner can burn additional fuel with the products from the turbine due to the presence of unconsumed oxygen in the upstream section of the jet engine [18]. When the afterburner is turned on, fuel is injected and the igniter is fired. As a result, the combustion process significantly increases the temperature of the afterburner outlet, which leads to a rapid increase in the engine net thrust [18].

The afterburner typically employs a bluff body as a flame holder to stabilise the flame and the V-gutter type is mainly used [19]. The V-gutter stabilises the flame by forming a recirculation zone at the downstream region, which lowers the flow speed. Many studies [20–27] examined the flame stabilisation mechanism using a bluff body for various fuels including the SAFs. Chaudhuri et al. [20] showed that the local flame extinction occurs when the high local stretch rates, which is caused by the overlap between the flame front and the shear layer vortices, exceeds the extinction stretch rates. Nair and Lieuwen [23] investigated the dynamics of a near-blowoff and bluff-body stabilised flame and found that these flames exhibit enhanced unsteadiness in two distinct stages before blowoff: (1) the holes in the flame sheet due to high instantaneous stretch rate and (2) the large-scale alterations of the wake dynamics, violent flapping of the flame front, and even larger straining of the flame. Tuttle et al. [24] investigated the flame holding and blowoff characteristics of bluff-body stabilised turbulent propane flames in vitiated premixed flows using in-tandem combustor. As the equivalence ratio decreased, they observed a higher occurrence of local extinctions along the flames interacting with shear layers surrounding the bluff body recirculation zone [24]. Furthermore, they revealed that the lean blowoff stability boundary for vitiated flows occurred at lower equivalence ratios compared to those in unvitiated flows with the same Reynolds number [24]. Pathania et al. [25] investigated the LBO behaviour of unconfined lean premixed bluff-body stabilised flames with various fuels including A-2 and C-1. They experimentally showed that A-2 and C-1 flames have higher *Le* compared to methane flames, resulting in lower extinction strain rates, and thus blowoff occurs at higher equivalence ratios for the same bulk velocity [25]. Mellor et al. [26, 27] showed that the LBO occurs when the residence time of the fresh mixture in the shear layer is less than the chemical time scale. Therefore, LBO occurs when the residence time of the fuel in the shear layer is smaller than the sum of evaporation time and ignition delay time [26–28].

Equation (1) shows the Damköhler number (Da) which is a dimensionless number representing the ratio of residence time scale to the chemical time scale [29].

$$\mathrm{Da} = \frac{\textit{residence time scale}}{\textit{chemical time scale}} = \frac{\tau_r}{\tau_c} \tag{1}$$

Husain [30] have proposed a residence time scale for bluff body flow as follows.

$$\tau_r = \frac{D}{U} \tag{2}$$

where D is a bluff body diameter and U is a characteristic velocity (lip velocity).

The ignition delay time (τ_i) can be used as the chemical time scale [31]. The ignition delay time can be measured as the time between the start of fuel injection and the start of significant heat release by ignition quality test (IQT) [32]. Gowdagiri et al. [33] identified that ignition delay time decreases as

https://doi.org/10.1017/aer.2024.49 Published online by Cambridge University Press

increasing the DCN. Also, many studies [33–37] have tried to figure out the correlation of ignition delay time with pressure, temperature, equivalence ratio, and DCN using three-Arrhenius model as follows.

$$\frac{1}{\tau_i} = \frac{1}{\tau_L + \tau_M} + \frac{1}{\tau_H} \tag{3}$$

$$\tau_j = A_j \left(\frac{P}{P_{ref}}\right)^{\alpha_j} \phi^{\beta_j} \left(\frac{\mathrm{DCN}}{\mathrm{DCN}_{ref}}\right)^{\gamma_j} exp\left(\frac{T_{act,j}}{T}\right) for\, j = L,\ M,\ H \tag{4}$$

where τ_j is the time constant, P_{ref} is a reference pressure, and DCN_{ref} is a reference DCN. A_j, α_j, β_j, γ_j, and $T_{act,j}$ are constant parameters chosen for each temperature range (subscripts L, M, and H represents low-, moderate-, and high-temperature, respectively) to fit experimental data. Here, each constant is varied depending on the fuel, but γ_j is negative or 0 for all targeted fuels. Therefore, the ignition delay time tends to decrease as DCN increases.

Wang et al. [38] showed that the global Da acts as an indicator of LBO. In other words, they found that LBO occurs if the global Da is less than unity. Furthermore, the previous studies [28, 39] confirmed that the combustion becomes more stable as the global Da increases.

In addition, since the turbine is installed after the combustor in a gas turbine engine, there are many efforts to prevent the failure caused by high temperature damage to turbine blades [40]. In particular, since the temperature of the combustion products is high, the dilution air is supplied to the downstream section of the main combustor to lower the temperature of the products [40]. Furthermore, since the afterburner is installed at the downstream end of the turbine, the flashback at the afterburner can cause high thermal damage to the turbine blades, so it is very important to understand the flashback characteristics of the bluff body flame. Jeong et al. [21] examined the characteristics of the flashback caused by the combustion instability and showed that the strong turbulence intensity due to the combustion instability increased the flashback distance.

As the replacement of jet fuel by SAF is required for military aircraft as well, it is important to understand the combustion characteristics of the SAF at the afterburner using a V-gutter, but existing research on this is not sufficient. Furthermore, to capture the characteristics of the afterburner, there should be the main combustor operated before the afterburner and the combustion products from the main combustor should be supplied to the afterburner as reactants. This is quite complicated to realise experimentally. As a result, the research on the two-staged combustor arranged in-tandem is relatively rare [24, 41]. Recently, as dry air or vitiated air was supplied in the first stage, combustion characteristics at the V-gutter in the second stage were studied using NJFCP test fuels [41]. However, the combustion condition at the first stage was not clear and also the flashback was not covered in the study.

Furthermore, combustion instability can lead to significant amplification of pressure perturbations inside the combustor, potentially causing damage to the engine or even explosions. Combustion instability is a phenomenon caused by the nonlinearity of combustion systems. Therefore, it is necessary to understand the nonlinear characteristics to identify the combustion instability characteristics. In many studies [42, 43], the phase-space of the pressure inside the combustion chamber has been used to identify the nonlinear dynamic characteristics and the presence of limit cycles from combustion instability. The phase-space can be represented by the time-delayed coordinates of the time series pressure perturbation as Equation (5).

$$\mathbf{X}(t_i) = (p'(t_i),\ p'(t_i - \tau),\ p'(t_i - 2\tau),\ \cdots,\ p'(t_i - (D-1)\tau)) \tag{5}$$

where $i = 0, 1, \cdots, n$ (n is the number of the time series pressure data), $\mathbf{X}(t_i)$ is the phase space vectors, $p'(t_i)$ is the pressure perturbation at time t_i, D is the dimension of the phase space, and τ is the time lag [43]. The time lag can be determined as the first zero-crossing when using the autocorrelation function, else, the time lag is chosen as the first minimum of the entropy when using the mutual information [43]. This study utilises the autocorrelation function, so the time lag is determined as the first zero-crossing.

The main purpose of this study is to investigate the combustion characteristics of the test SAFs including the LBO, flashback, and combustion instability at the in-tandem combustor with the afterburner,

https://doi.org/10.1017/aer.2024.49 Published online by Cambridge University Press

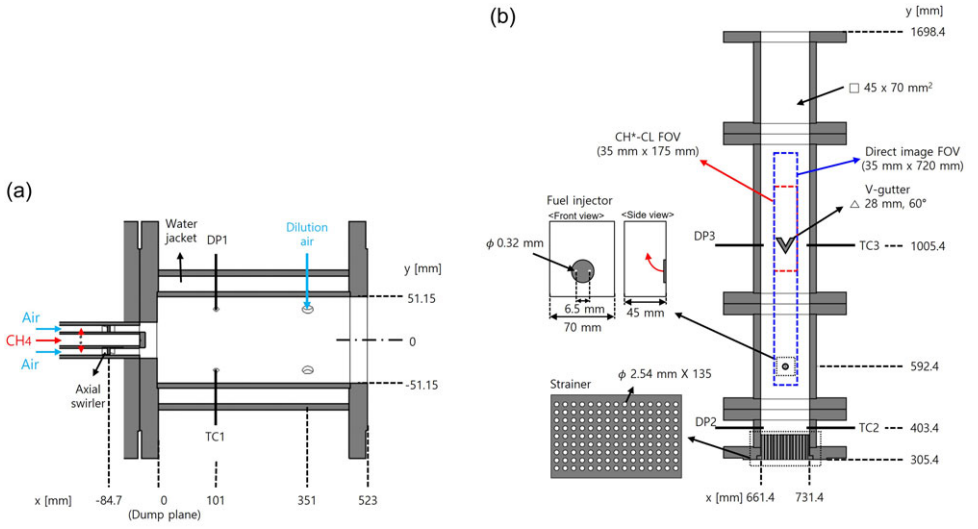

Figure 1. *Schematic of the in-tandem combustor: (a) the main combustor with swirler and (b) the afterburner with V-gutter.*

which can help accelerate the use of SAF. Specifically, this study examines the combustion characteristics at the afterburner, which receives the combustion products as the reactants, using the in-tandem combustor and investigates the flashback characteristics of test SAFs.

The remainder of this paper is organised as follows. We first describe the experimental method and test fuel properties. Next, we present the LBO and flashback characteristics, effect of shear layer reactivity on flame characteristics, and combustion instability characteristics. Finally, conclusions, limitations, and future directions for the work are provided.

2.0 Experiment methods

2.1 Two-staged in-tandem combustor

In this study, a scaled-down experimental test rig is designed and used to capture the main characteristics of the afterburner by feeding the combustion products from the main combustor to the afterburner. Figure 1 shows an in-tandem combustor with a main combustor and an afterburner used in this study. As shown in Fig. 1(a), the horizontal main combustor has a circular cross-section with a radius of 51.15 mm. The length of the main combustor is 523 mm, and the main combustor is connected to the afterburner by a 90 degree elbow. The water jacket around the main combustor prevents the thermal damage to the main combustor. Air and methane are used as the oxidiser and fuel, respectively, for the main combustor. The air and methane are mixed as jets-in-crossflow and the mixture passes through an axial swirler before entering the main combustor. The swirler has a diameter of 35 mm and has 10 swirl vanes with a swirl angle of 30 degrees. At the downstream end of the main combustor, dilution air is introduced to lower the temperature of the combustion products from the main combustor and to supply additional oxidiser for the afterburner. One dynamic pressure sensor (DP1) and one temperature sensor (TC1) are installed at the upstream end of the main combustor.

Figure 1(b) shows the afterburner which is installed on the 90 degree elbow vertically. The afterburner is composed of a flow strainer and three modules, and the rectangular cross-section of the afterburner is 45×70 mm^2. The flow strainer is a plate with 135 holes with a diameter of 2.54 mm and is used to reduce the flow inhomogeneity caused by the 90 degree elbow. The afterburner uses the combustion products from the main combustor and dilution air as reactants and the liquid test fuel is additionally

https://doi.org/10.1017/aer.2024.49 Published online by Cambridge University Press

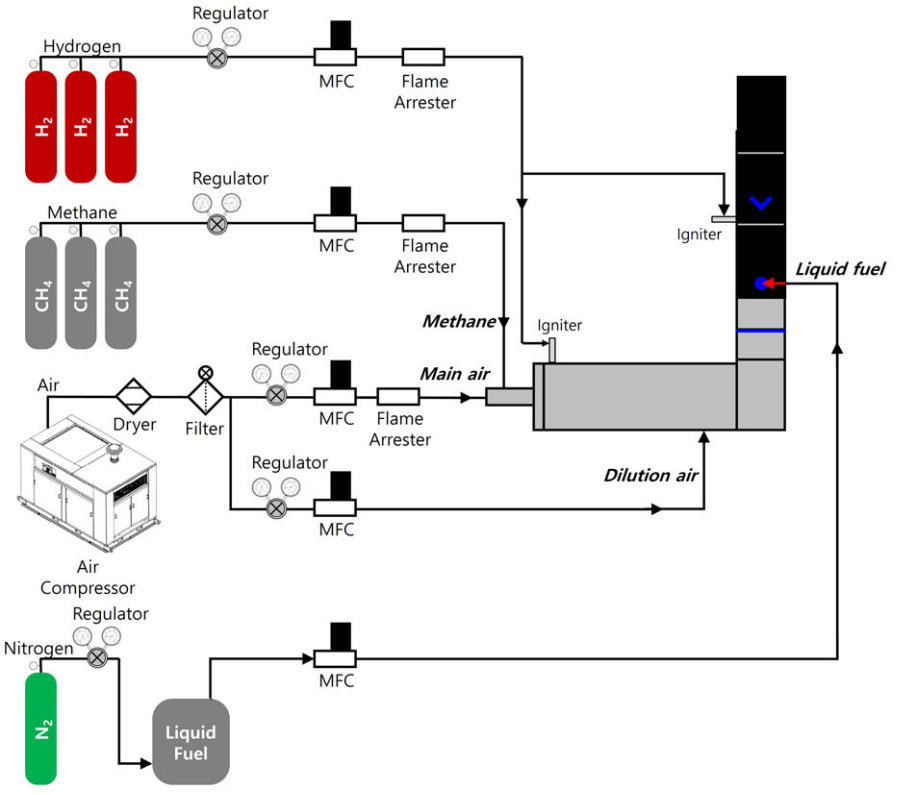

Figure 2. *Schematic of the experimental setup.*

introduced at the upstream section of the afterburner as reactant. The length of the afterburner is about 1,400 mm and the downstream end of the afterburner is set as an acoustic open boundary condition. The liquid test fuel injector at the first module of the afterburner consists of two holes with 6.5 mm apart on the top of the injector and the orifice diameter is 0.32 mm. Both holes are oriented perpendicular to the cross-flow direction, so the liquid test fuel and the products from the main combustor are mixed as jets-in-crossflow. The flame holder at the second module is a V-gutter type with a vertex angle of 60° and a side length of 28 mm. The flame holder's blockage ratio (V-gutter width/test section width) is 40%. The flame holder is placed 413 mm downstream after the liquid test fuel injector. Hydrogen torch igniters are mounted upstream end of the main combustor and before the flame holder to ignite the flames, respectively. Two quartz windows are employed on each sidewall on the two modules for optical access for the test fuel injector and the flame holder, respectively.

2.2 Experimental setup

Figure 2 shows the schematics of the experimental setup for this study. The air is provided from the compressor (SULLAIR, 4509AC) and controlled by a mass flow controller (MFC) (Brooks, SLA5853S, uncertainty = ± 0.6% of set point). The methane and hydrogen are provided from each bottle of high-purity feedstock gases (CH_4 purity > 99.99 mol% and H_2 purity > 99.999 mol%) and controlled by MFC (Brooks, SLA5851S, uncertainty = ± 0.6% of set point). Air, methane, and hydrogen are supplied to the combustor at room temperature (290 ± 5 K). The liquid test fuel is provided from the N_2 pressurised tank and also controlled by MFC (Alicat, KC-1K, uncertainty = ± 0.2% of set point).

https://doi.org/10.1017/aer.2024.49 Published online by Cambridge University Press

Table 1. *Characteristics of test fuels used in this study [1, 6, 45]*

Test fuels	DCN (Derived cetane number)	HOC (MJ/kg) (Heat of combustion)	MW (kg/kmol) (Molecular weight)
Jet-A	48.3	43.1	159.0
A-2	48.3	43.1	159.0
C-1	17.1	43.8	178.0
C-5	39.6	43.0	135.0
C-9	63.3	44.0	174.5
JP-8/HRJ	52.5	43.9	160.1

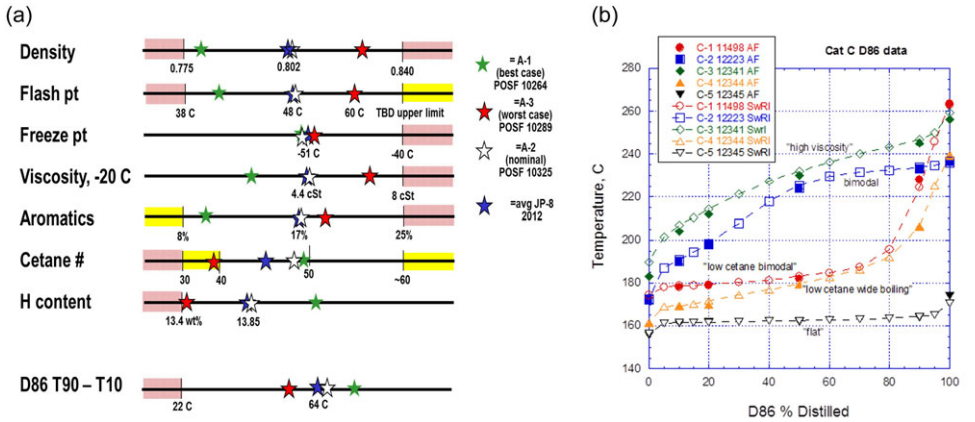

Figure 3. *(a) Test fuel properties of category A fuels and (b) distillation curves for category C fuels [1].*

2.3 Liquid test fuel characteristics

The research using NJFCP test fuels focuses on the characteristics of two types of test fuels: category A and C. Category A fuels represent conventional petroleum-derived fuels with typical properties (viscosity, flash point, aromatic content, etc.) [44]. On the other hand, category C fuels are experimental fuels specifically designed to explore the extreme boundaries of jet fuel composition and properties [44]. Due to their distinct physical and chemical properties, each test fuel exhibits variations in combustion characteristics such as lean blowoff, flashback, and combustion instability.

This study investigates the combustion characteristics of a total of five NJFCP test fuels (Jet-A, A-2, C-1, C-5, and C-9) and a JP-8/HRJ. A total of six fuel samples were prepared by the National Research Council (NRC). Table 1 shows the characteristics of each test fuel. Each test fuel has similar heat of combustion, but with a DCN difference of up to 3.7 times. Figures 3(a) and (b) show the properties of category A fuels and the distillation curves for category C fuels, respectively. A-2 is a test fuel with the average value of Jet-A characteristics. C-1 has a very low cetane number. C-5 has a flat boiling point. C-9 is a mixture of 80% hydrotreated renewable jet (HRJ) biofuel and 20% dodecane, and JP-8/HRJ is a mixture of 50% HRJ and 50% Jet-8.

2.4 Experimental conditions

Table 2 shows the detailed experimental conditions of this study. The flow rate of air and methane used at the main combustor are kept constant at 1,000 and 69.45 slpm, respectively, so that the equivalence ratio is kept at 0.66. The test SAF supplied to the afterburner is kept at 1,500 g/h, and the equivalence ratio at

https://doi.org/10.1017/aer.2024.49 Published online by Cambridge University Press

Table 2. *Experimental test conditions*

Parameters	Value	Unit
Main air flow rate	1,000	slpm
Main CH_4 flow rate	69.45	slpm
Dilution air flow rate	50–500	slpm
Liquid test fuel flow rate	1,500	g/h

the second stage burner is controlled as the dilution air flow rate is changed from 50 to 500 slpm. The inlet pressures of the air, methane, SAF, and dilution air are ambient condition. The inlet temperature of the afterburner is approximately 1,100 K, and this varies depending on the amount of dilution air.

2.5 Measurement and diagnostics

Three dynamic pressure sensors (DPs) (PCB, 112A22, uncertainty = ± 1% of full scale) and three thermocouples (TCs, K-type) are used to measure the pressure perturbation and temperatures, respectively, at the main combustor, after the flow strainer, and at the flame holder. The dynamic pressure sensors and thermocouples are operated at 10 kHz and 10 Hz rates, respectively. To prevent thermal damage to the TCs, temperatures near the wall were measured within the temperature range suitable for K-type TCs.

The global OH^*-chemiluminescence (CL) intensity near the flame holder is measured by a photomultiplier tube (PMT) (Hamamatsu, H11526-20-NF) at 10 kHz rates. CH^*-CL images are captured at 10 Hz with an intensified charged-coupled device (ICCD) camera (Princeton Instruments, PI-MAX) using a UV-enhanced lens (LaVision, $f = 100$ mm, f/2.8) with a 430 nm bandpass filter. Direct images are obtained using a digital single-lens reflex (DSLR) camera (Nikon, D750). The fields of view (FOVs) of the CH^*-CL and direct images are 35 mm × 175 mm and 35 mm × 720 mm, respectively, as denoted in Fig. 1.

3.0 Results and discussion

3.1 Lean blowoff (LBO) and flashback characteristics

In the following, we present and discuss comparative results of the six sample fuels. The characteristics of LBO and flashback are identified by varying the global equivalence ratio at the afterburner (ϕ_{af}), while keeping the condition for the main combustor the same. In Fig. 4, the operational limits of each test fuel are presented in the order of its DCN. It clearly shows the implications regarding the significance of DCN on the LBO and flashback characteristics.

Figure 5 shows the LBO equivalence ratio for each test fuel. Blowoff occurs when the flow residence time scale is less than the chemical time scale. Since the flame speed decreases and the flow speed increases as decreasing ϕ_{af} (by increasing the dilution air flow rate) in this study, the possibility of blowoff increases as decreasing ϕ_{af}. The LBO occurs at ϕ_{af} of about 0.42 for the C-1 with the lowest DCN in this study, but the LBO equivalence ratio decreases for the test fuel with higher DCN and LBO occurs at ϕ_{af} of about 0.3 for the C-9 with the highest DCN in this study.

The DCN is a chemical property of fuels [15] and the DCN indicates the chemical reactivity potential [46, 47]. Therefore, a small DCN means a high chemical time scale [33] and a low Da under the same residence time scale according to Equation (1). According to the previous studies [33, 34], the chemical time scale is lower for higher DCN fuel. Also, in previous studies [32, 48], the relational expression between the ignition delay time (τ_i) of diesel fuel and DCN was identified within the range of ignition delay time of 3.1–6.5 ms, which is shown in Equation (6).

https://doi.org/10.1017/aer.2024.49 Published online by Cambridge University Press

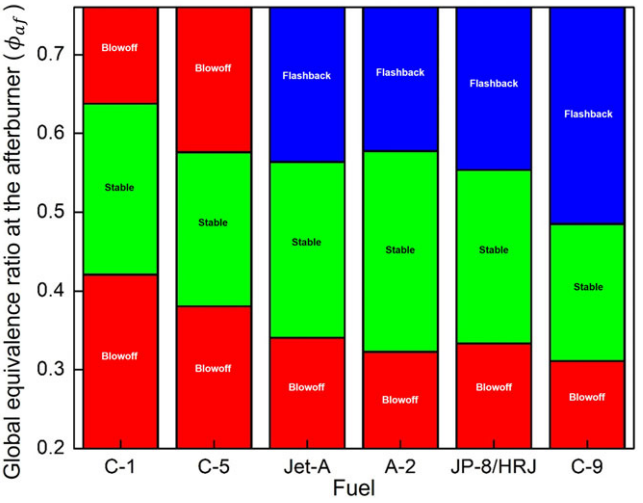

Figure 4. *Operational limits of each test fuel.*

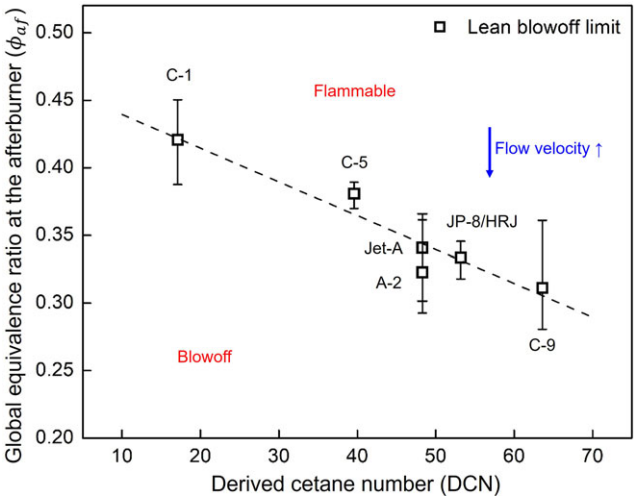

Figure 5. *ϕ_{af} at the lean blowoff (LBO) for each test fuel.*

$$DCN = 83.99(\tau_i - 1.512)^{-0.658} + 3.547 \tag{6}$$

Since Equation (6) was derived for diesel fuels comprising ASTM National Exchange Group (NEG) check fuels, heptamethylnonane, cetane, and an in-house check fuel [48] at 2.137 MPa and 545 °C, it is difficult to apply it directly to our cases, but it can be seen that ignition delay time is closely related to DCN. However, research on the ignition time for NJFCP test fuels is not sufficient yet.

Since the total flow rate is kept same regardless of the test fuel at the same ϕ_{af}, there will be almost no change in the residence time as shown in Equation (2). Therefore, in our case, Da number will increase with the increase of DCN as chemical time scale decreases (ignition delay time decreases) and residence time is almost constant.

In other words, test fuels with a small DCN are more easily blown-off. As shown in Fig. 5, the LBO equivalence ratio decreases as the DCN increases since the flame can be sustained even at a faster flow speed due to a small chemical time scale, which is consistent with the results of previous studies.

https://doi.org/10.1017/aer.2024.49 Published online by Cambridge University Press

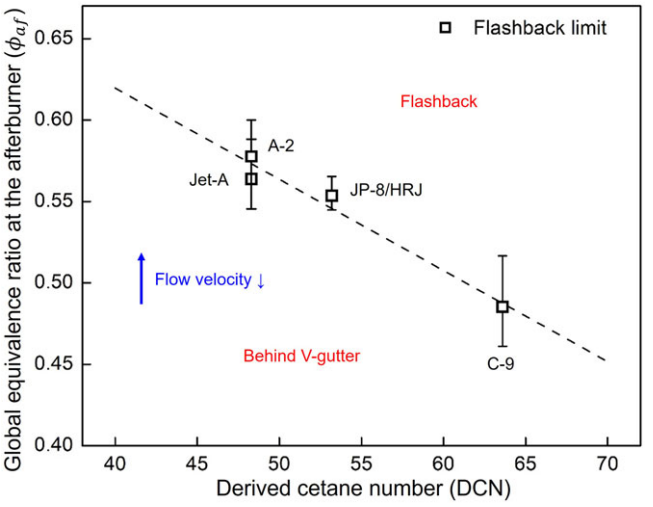

Figure 6. *ϕ_{af} at the onset of the flashback for each test fuel.*

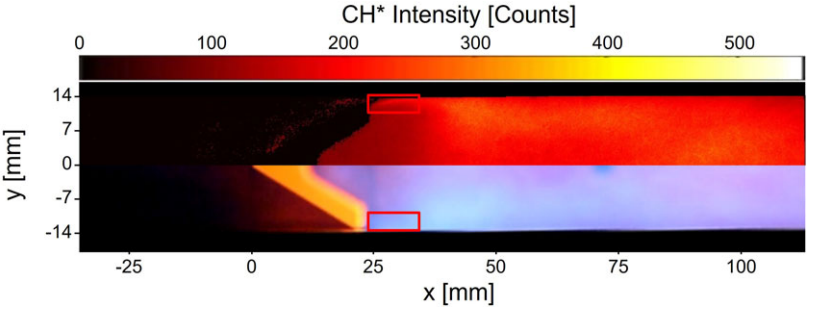

Figure 7. *CH*-CL image (upper) and direct image (lower) of A-2 under $\phi_{af} = 0.6$.*

Figure 6 shows ϕ_{af} when flashback occurs for each test fuel. Flashback occurs when the flame speed is faster than the flow speed. In this study, the flashback propensity increases as ϕ_{af} increases by decreasing the dilution air flow rate since the flame speed increases and the flow speed decreases. Here, for C-9 with the highest DCN in this study, flashback occurs at ϕ_{af} of about 0.48. However, for test fuels with lower DCN, flashback occurs at a higher ϕ_{af}. This indicates that flashback has a strong correlation with DCN in a similar way to blowoff, which has not been discussed in previous studies.

Behind the V-gutter, the flow speed is low owing to the recirculation zone, resulting in high Da and stable flame. However, for flashback to occur, flames need to propagate toward the upstream direction of V-gutter, where the flow speed is fast. Therefore, flow time scale becomes smaller, so Da becomes smaller, resulting in a high possibility to be extinguished. Since the fuel with a high DCN has a small chemical time scale, even if the flow time scale becomes smaller, the flame can be sustained and flashback can occur. Therefore, the flashback of C-9 flame with the highest DCN in this study occurs at a faster flow speed and the flashback of test fuels with lower DCN occurs at a lower flow speed. However, for the flames by the C-1 and C-5 test fuels with even smaller DCNs, blowoff occurs instead of flashback. This will be discussed later.

https://doi.org/10.1017/aer.2024.49 Published online by Cambridge University Press

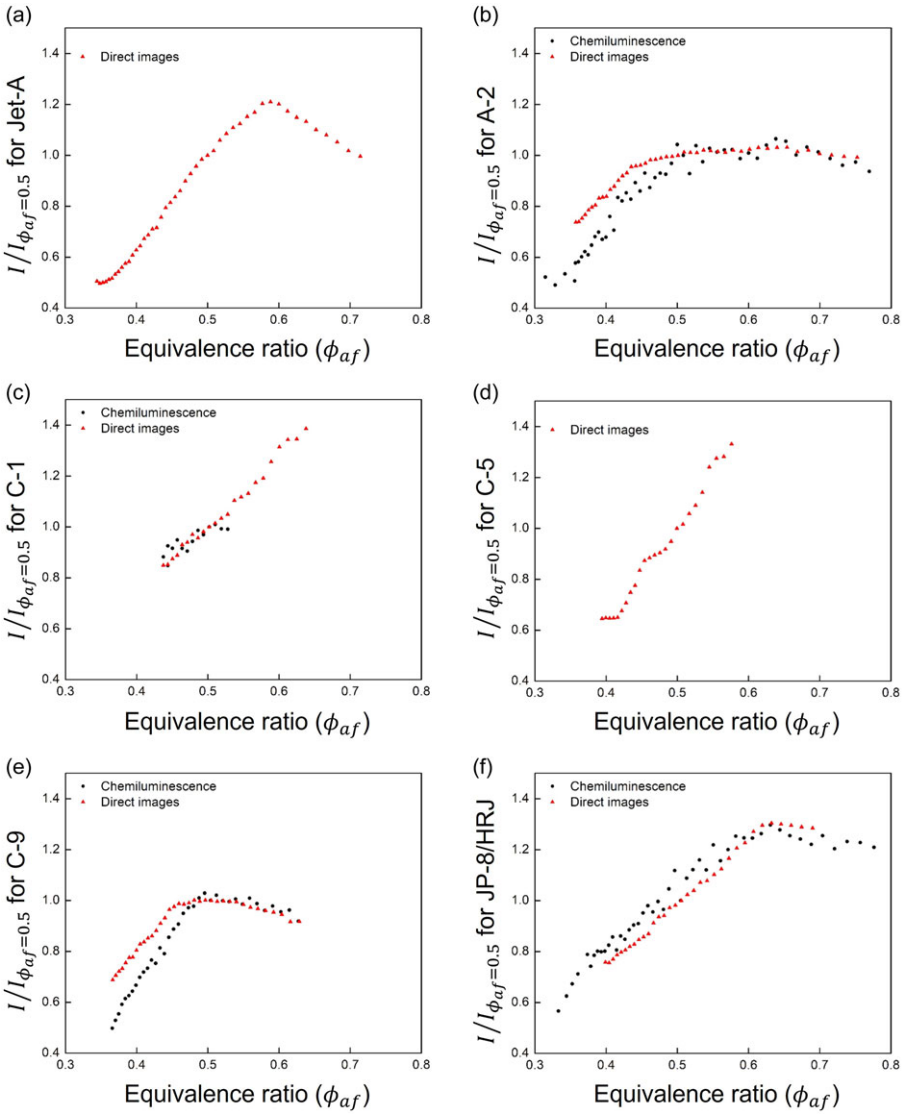

Figure 8. *Relative shear layer reactivity standardised using $I_{\phi_{af}=0.5}$ of (a) Jet-A, (b) A-2, (c) C-1, (d) C-5, (e) C-9, and (f) JP-8/HRJ.*

3.2 Effect of shear layer reactivity on flame characteristics

The flame at the afterburner in this study is anchored to the V-gutter which acts as a flame holder. According to the previous study [14, 20, 49, 50], the shear layer at the V-gutter tip has a strong influence on the stability and characteristics for the bluff body flame. Despite the ongoing debate surrounding the efficacy of CH^* as a reliable indicator for accurately assessing the local heat release rate or reactivity [51, 52], it remains a good marker commonly utilised in numerous studies [52, 53]. Consequently, this study also incorporated CH^* as an indicator to evaluate shear layer reactivity. To examine the reactivity of the shear layer, the ratio of image intensity inside the red box shown in Fig. 7 to that of the averaged total flame is calculated as shown in Equation (7).

$$I = \frac{intensity\ of\ red\ box}{average\ intensity\ of\ flame} \tag{7}$$

https://doi.org/10.1017/aer.2024.49 Published online by Cambridge University Press

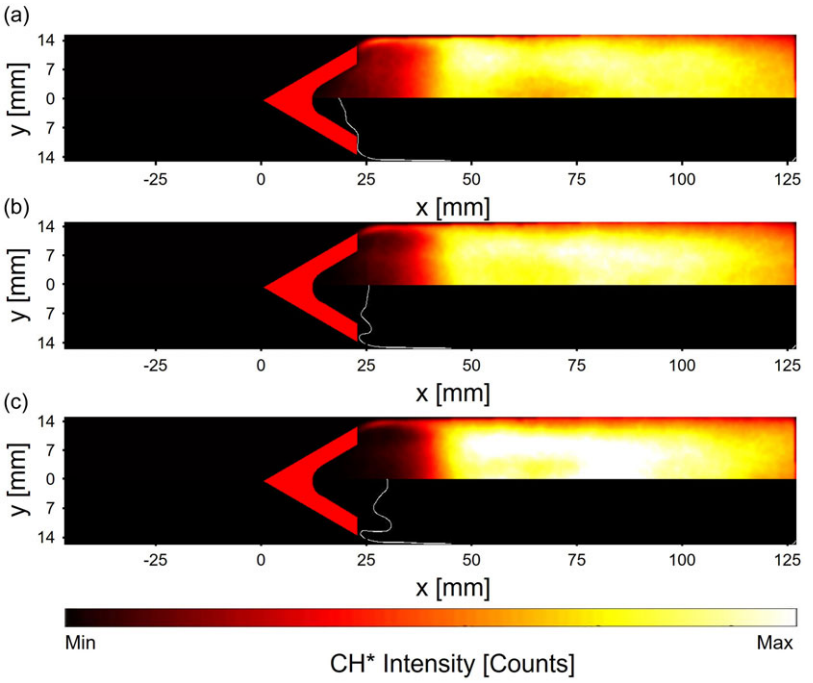

Figure 9. *The changes in averaged A-2 fueled flame shape according to the global equivalence ratio at the afterburner: (a) $\phi_{af} = 0.47$, (b) $\phi_{af} = 0.41$, and (c) $\phi_{af} = 0.36$.*

I represents the relative reactivity in the shear layer compared to the average total flame. Therefore, a high I corresponds to a case where the flame is concentrated in the shear layer region and is strongly anchored to the V-gutter. Here, since the I is calculated using both CH*-CL and direct images because of the FOV limitation and lack of CH*-CL data due to operational constraints of the experimental setup and test fuels, the I is standardised by the I at ϕ_{af} of 0.5 to compare the results from both of them.

Figure 8 shows the shear layer reactivity standardised by the I at ϕ_{af} of 0.5 ($I/I_{\phi_{af}=0.5}$). As shown in Fig. 8, it shows a trend that the value of $I/I_{\phi_{af}=0.5}$ decreases as ϕ_{af} decreases when the equivalence ratio is below a certain specific value to each fuel, indicating that the flame anchoring at the V-gutter is weakened. In other words, as the combustion condition approaches to a leaner condition by decreasing ϕ_{af}, the flame speed decreases and the flow speed increases, resulting in a decrease in Da. Therefore, the flame anchoring to the V-gutter is weakened, eventually causing blowoff.

Figure 9 shows the change in the average flame shape as decreasing the ϕ_{af} for the A-2 flame. The upper side of Fig. 9 shows the CH*-CL image and the bottom side of Fig. 9 shows the flame edge obtained through Sobel edge detection of the upper side image. It can be seen that the average flame front is gradually pushed downstream as the ϕ_{af} decreases. In other words, as the ϕ_{af} decreases, the $I/I_{\phi_{af}=0.5}$ decreases and the average flame front is also pushed downstream, so when the ϕ_{af} becomes lower, it can be seen that the flame blowoff occurs by detaching from the V-gutter.

In contrast, as the ϕ_{af} increases, Da increases and the flame is better anchored to the V-gutter, increasing the shear layer reactivity. However, the shear layer reactivity of Jet-A, A-2, C-9, and JP-8/HRJ flames tends to decrease after a certain ϕ_{af} due to the occurrence of flashback as shown in Fig. 8. When flashback happens, the reactivity of the shear layer is weakened because the reactants are already reacted before reaching the shear layer. Since flashback does not occur in C-1 and C-5 flames, the shear layer reactivity does not decrease as the ϕ_{af} increases. Figure 10 shows the change in the average flame shape as increasing the ϕ_{af} for the A-2 flame. As in Fig. 9, the upper side and bottom side of Fig. 10 show

https://doi.org/10.1017/aer.2024.49 Published online by Cambridge University Press

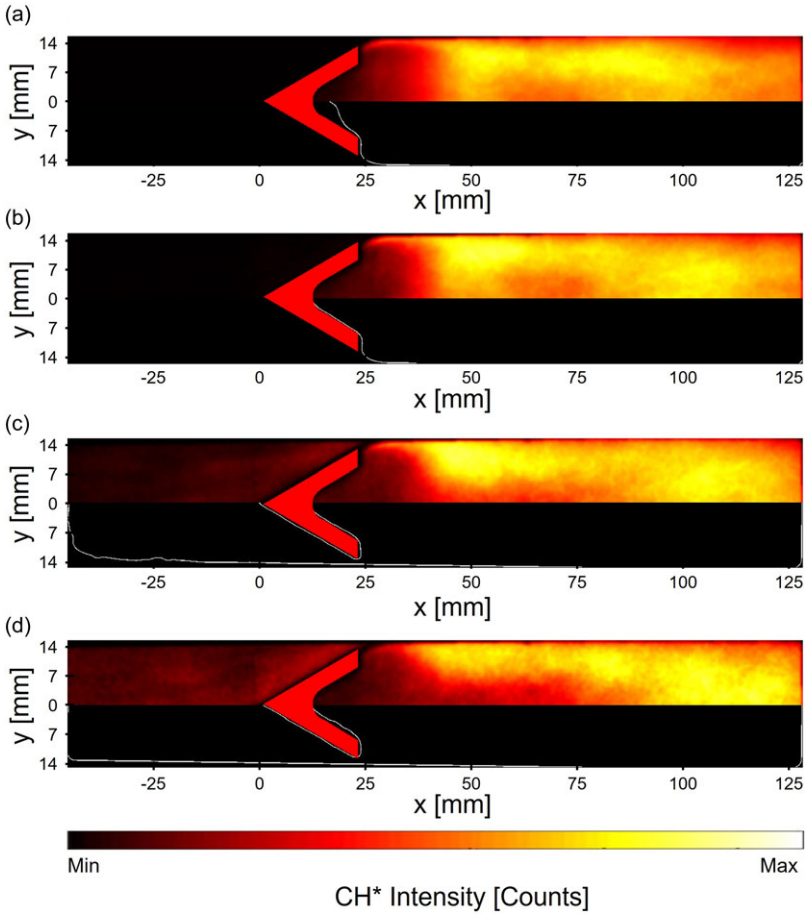

Figure 10. *The changes in averaged A-2 fueled flame shape according to the global equivalence ratio at the afterburner: (a) $\phi_{af} = 0.48$, (b) $\phi_{af} = 0.58$, (c) $\phi_{af} = 0.68$, and (d) $\phi_{af} = 0.77$.*

the CH*-CL image and the edge of the flame, respectively. As the ϕ_{af} increases, the flame front shifts upstream, eventually leading to flashback.

Figure 11 shows the relationship between the ϕ_{af} where flashback occurs and the ϕ_{af} where the $I/I_{\phi_{af}=0.5}$ is the maximum in Fig. 8. It can be seen that the two ϕ_{af} have a proportional relationship and the shear layer reactivity and flame shape are closely related. However, shear layer reactivity was not measured under all combustible ϕ_{af} for all fuels, so additional measurement and analysis are needed in future work.

3.3 Combustion instability characteristics

With the increase of the ϕ_{af}, the flame speed increases, while the flow speed decreases due to reduced dilution air, so Da increases and the likelihood of blowoff decreases. Indeed, for the flames by Jet-A, A-2, C-9, and JP-8/HRJ test fuels, as the ϕ_{af} increases, blowoff does not occur until flashback occurs. However, as mentioned in Chapter 3.1, for flames using C-1 and C-5 test fuels, blowoff occurs before flashback occurs as ϕ_{af} increases. This is deemed to be related to the pressure perturbation. As can be seen in Fig. 1, pressure perturbations (p_2' and p_3') are measured by a high frequency pressure transducers ported just after the honeycomb (DP2) and near the V-gutter (DP3). p_2' is the pressure perturbation upstream end of the afterburner, which represents the pressure perturbation affecting the turbine blade, and p_3' is the pressure perturbation near the V-gutter, which is closely related to the heat release rate

https://doi.org/10.1017/aer.2024.49 Published online by Cambridge University Press

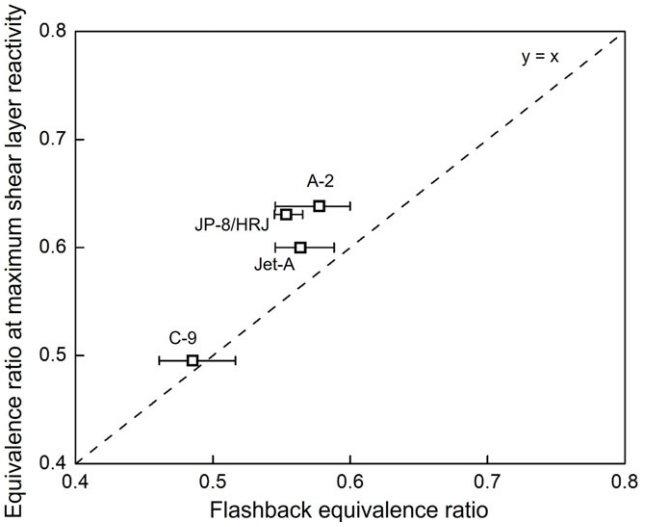

Figure 11. *Relationship between ϕ_{af} where the shear layer reactivity is highest and ϕ_{af} where the flashback occurs.*

fluctuation from the flame at the afterburner. Therefore, p_2' and p_3' were measured and analysed for the strength of pressure perturbation and the phase difference between the pressure perturbation and the heat release rate fluctuation, respectively.

Figure 12 shows the pressure perturbations (p_2' and p_3') according to the change in the ϕ_{af} for each test fuel. The plots are obtained by varying the dilution air flow rate while maintaining a steady liquid test fuel flow. The RMS pressures start with the low RMS pressure at the low ϕ_{af} for all test fuels, then rapidly increase with the increase in the ϕ_{af} until they reach a plateau region or blowoff. This is similar to the results of previous studies [54, 55], which examined the pressure perturbations for some NJFCP test fuels and found that pressure perturbation increased sharply above a certain equivalence ratio. For comparison among test fuels, curve fits are performed for the RMS pressures of A-2 and these curve fits are plotted in the red and blue lines along with the RMS pressures. It can be seen that C-1 and C-5 flames have notably different tendency between the RMS pressures and the ϕ_{af} while other test fuels show similar trend. In overall, they show much higher RMS pressures compared to other test fuels. In addition, C-1 and C-5 flames don't have flat RMS pressure region at the low ϕ_{af} because they are blown off at higher ϕ_{af} than other test fuels. They are also blown off at a high ϕ_{af} of near 0.64 and 0.58 before flashback happens, respectively. Therefore, flammability limit for C-1 and C-5 flames are narrower than that of the other test fuels.

Figure 13 shows the three-dimensional phase space of A-2 flame obtained from p_2' for different ϕ_{af}. When ϕ_{af} is 0.32, the trajectories fill the core of the phase space, which means p_2' does not have deterministic dynamic characteristics. With the increase of ϕ_{af}, it is clearly seen that the trajectory deviates from the core of the phase space and limit cycle is formed. This indicates that the periodicity of the dominant pressure perturbations becomes stronger. This trend happens similarly for all test fuels including C-1 and C-5 universally.

In addition, Rayleigh index, which represents the relationship between the pressure perturbation and the heat release fluctuations, is calculated by Equation (8). Here, both the pressure perturbation (p_3') and the heat release rate fluctuation (q') for calculating the Rayleigh index are measured near the V-gutter, where t_p is the period of oscillation.

$$\text{Rayleigh index} = \frac{1}{t_p}\int_0^{t_p} p_3'(t)\cdot q'(t)dt \tag{8}$$

https://doi.org/10.1017/aer.2024.49 Published online by Cambridge University Press

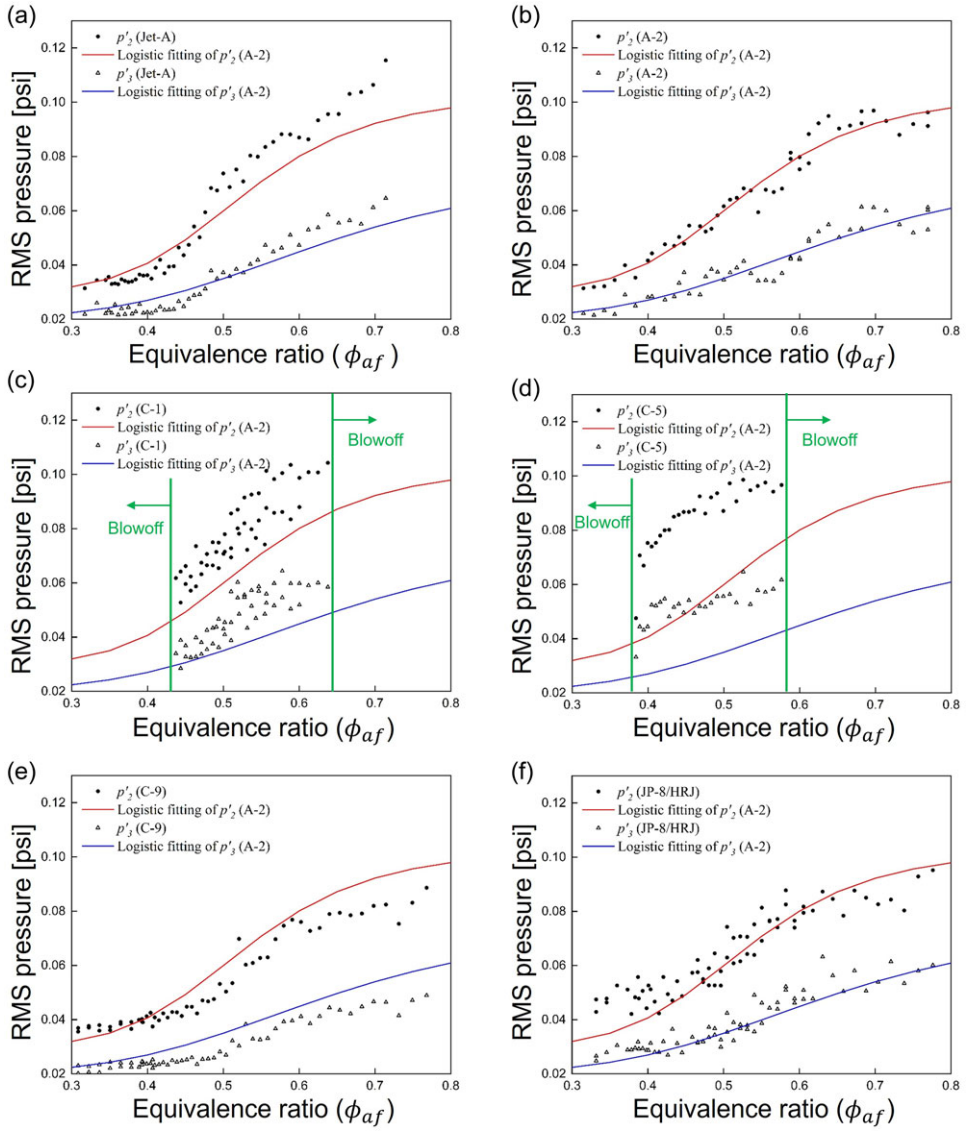

Figure 12. *RMS pressure perturbations measured just after the honeycomb (p'_2) and near the V-gutter (p'_3) for each of the test fuels ((a) Jet-A, (b) A-2, (c) C-1, (d) C-5, (e) C-9, and (f) JP-8/HRJ) according to the ϕ_{af} along with the curve fits of the RMS pressures for the A-2 test fuel (shown as the red and blue lines).*

As shown in Fig. 14, as the Rayleigh index increases, the strength of pressure perturbation also increases. The Rayleigh index refers to the degree of interaction between the pressure perturbation inside the afterburner and the heat release rate fluctuation. Therefore, the pressure perturbations shown in Fig. 12 are attributed to the thermo-acoustic combustion instability. Especially, the Rayleigh indexes of C-1 and C-5 are mostly positive and greater than those of other test fuels, which means that the strength of combustion instability of C-1 and C-5 flames is stronger than that of other flames. Therefore, as the equivalence ratios increase, C-1 and C-5 flames show strong combustion instability caused by constructive interference between the pressure perturbation and the heat release rate fluctuation leading to blowoff.

https://doi.org/10.1017/aer.2024.49 Published online by Cambridge University Press

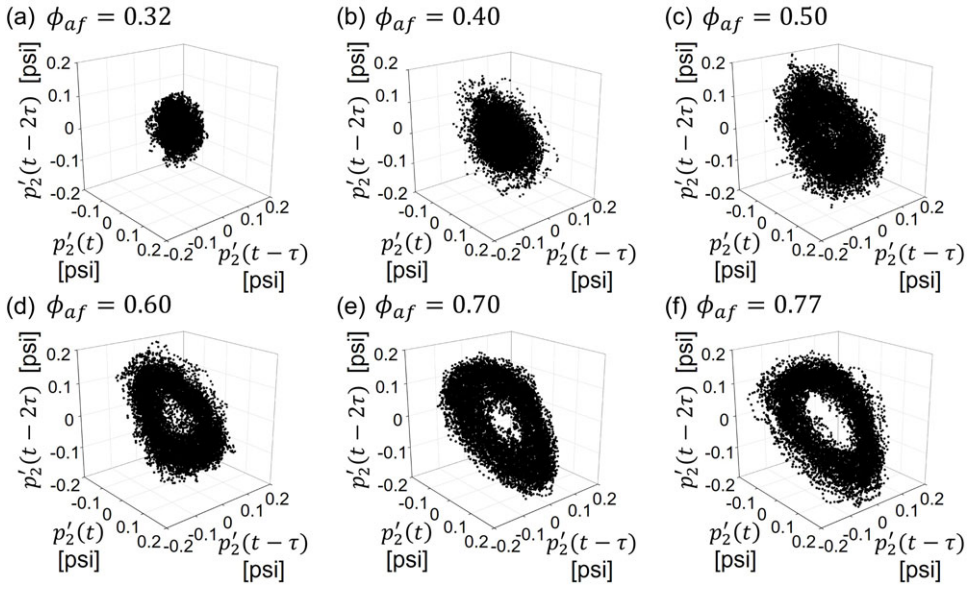

Figure 13. *Three-dimensional phase space [$p_2'(t)$, $p_2'(t-\tau)$, $p_2'(t-2\tau)$] for different ϕ_{af} using A-2.*

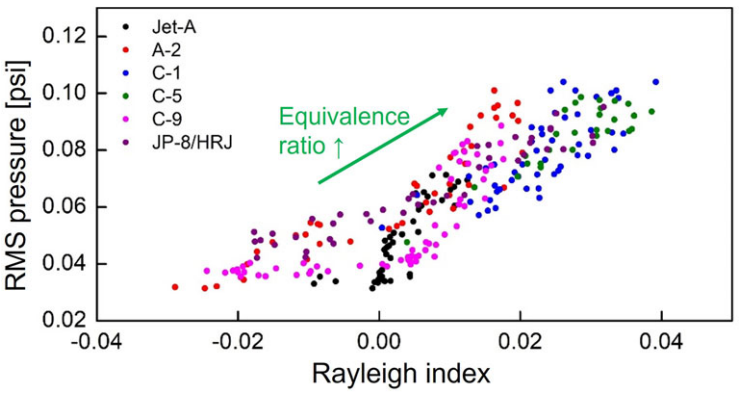

Figure 14. *RMS of p_2' for each of the test fuels according to the Rayleigh index.*

Figure 15 shows the RMS of p_2' according to the phase difference between the pressure perturbation (p_3') and the heat release rate fluctuation (q') for each test fuel. As shown in Fig. 15, RMS of p_2' is strong when the phase difference between p_3' and q' is near zero. Therefore, it can be also seen that the perturbation inside the afterburner is caused by the thermo-acoustic combustion instability.

Figure 16 shows the joint probability density distribution between the pressure perturbation at DP3 and the heat release rate fluctuation measured by PMT for each test fuel at the ϕ_{af} of 0.58. For the flames by Jet-A, A-2, C-9, and JP-8/HRJ test fuel, the distribution of p_3' and q' is circular in the centre and the order of the coefficient of linear relationship corresponds to O(-2). However, for the flames by C-1 and C-5, the distribution shows an upward-sloping trend and the order of the coefficient of linear relationship corresponds to O(-1). In other words, the interaction between the pressure and heat release rate perturbations is weak for the flames by Jet-A, A-2, C-9, and JP-8/HRJ, so perturbations are not strong. However, for the flames by C-1 and C-5, the interaction is stronger so the pressure and heat release rate perturbations are amplified strongly. In other words, the combustion instability occurs

https://doi.org/10.1017/aer.2024.49 Published online by Cambridge University Press

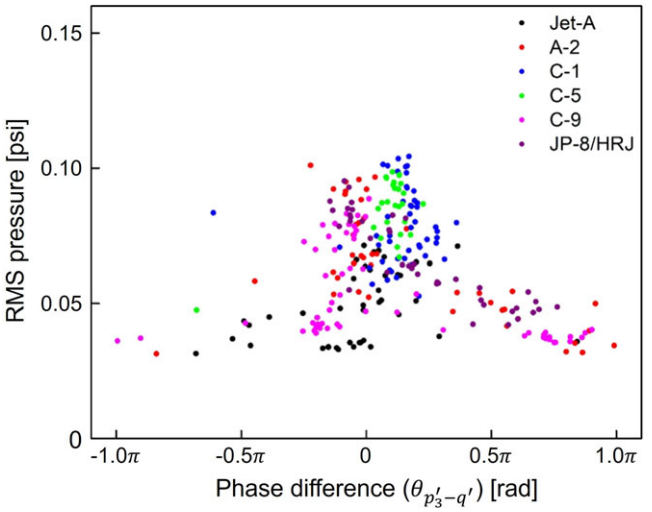

Figure 15. *RMS of p_2' according to the phase difference for each test fuel.*

strongly for C-1 and C-5 flames due to the relatively strong interaction between the pressure perturbation and the heat release rate fluctuation at the high ϕ_{af}, which makes the flame detach from the V-gutter and eventually causes the blowoff. In contrast, the flames by Jet-A, A-2, C-9, and JP-8/HRJ test fuels can be sustained without the blowoff even at the high ϕ_{af} since the interaction between the pressure perturbation and heat release rate fluctuation is weak and the DCN of the flames is also high.

Using chemiluminescence images of A-2, C-1, C-9, and JP-8/HRJ test fuel flames, the intensity centre within the chemiluminescence FOV was measured. Figure 17 shows the phase difference between pressure and heat release rate with respect to the intensity centre. The intensity centre is set at zero at the position of the V-gutter tip, with the upstream direction being positive and the downstream direction being negative. As the equivalence ratio increases, the intensity centre moves closer to the V-gutter tip. As shown in Fig. 17, as the intensity centre moves upstream, the phase difference between pressure perturbation and heat release rate fluctuation decreases. This is because the delay time between pressure perturbation and heat release rate fluctuation changes as the distance between the fuel injector and flame centre changes according to the equivalence ratio [56, 57]. Additionally, when the position of the intensity centre was around -30 mm, the phase difference was close to zero for all test fuels. For C-1 flame, the intensity centre was mostly located at -30 mm under most chemiluminescence measurement conditions, indicating a stronger oscillation intensity compared to other test fuels since the phase difference was close to zero.

4.0 Conclusion

Combustion characteristics of the test sustainable aviation fuels (SAFs) are experimentally explored using an in-tandem combustor. The main combustor operates with CH_4 and air, while the afterburner uses the combustion products of the main combustor, the dilution air, and the test SAF as reactants. A total of six test SAFs are used in this study. The following conclusions are drawn from our results.

The lean blowoff (LBO) and flashback characteristics of the test SAF flames are assessed with varying the global equivalence ratio at the afterburner (ϕ_{af}). The current study confirms, for the first time, that the flashback is also closely correlated to the derived cetane number (DCN) of each test fuel in a way similar to LBO. For the test fuels with higher DCN, the LBO and flashback occur at the lower ϕ_{af}. This is because fuels with higher DCN result in a lower chemical time scale for the flame, allowing it to be sustained under conditions of lower flow timescale (i.e., the faster flow speed).

https://doi.org/10.1017/aer.2024.49 Published online by Cambridge University Press

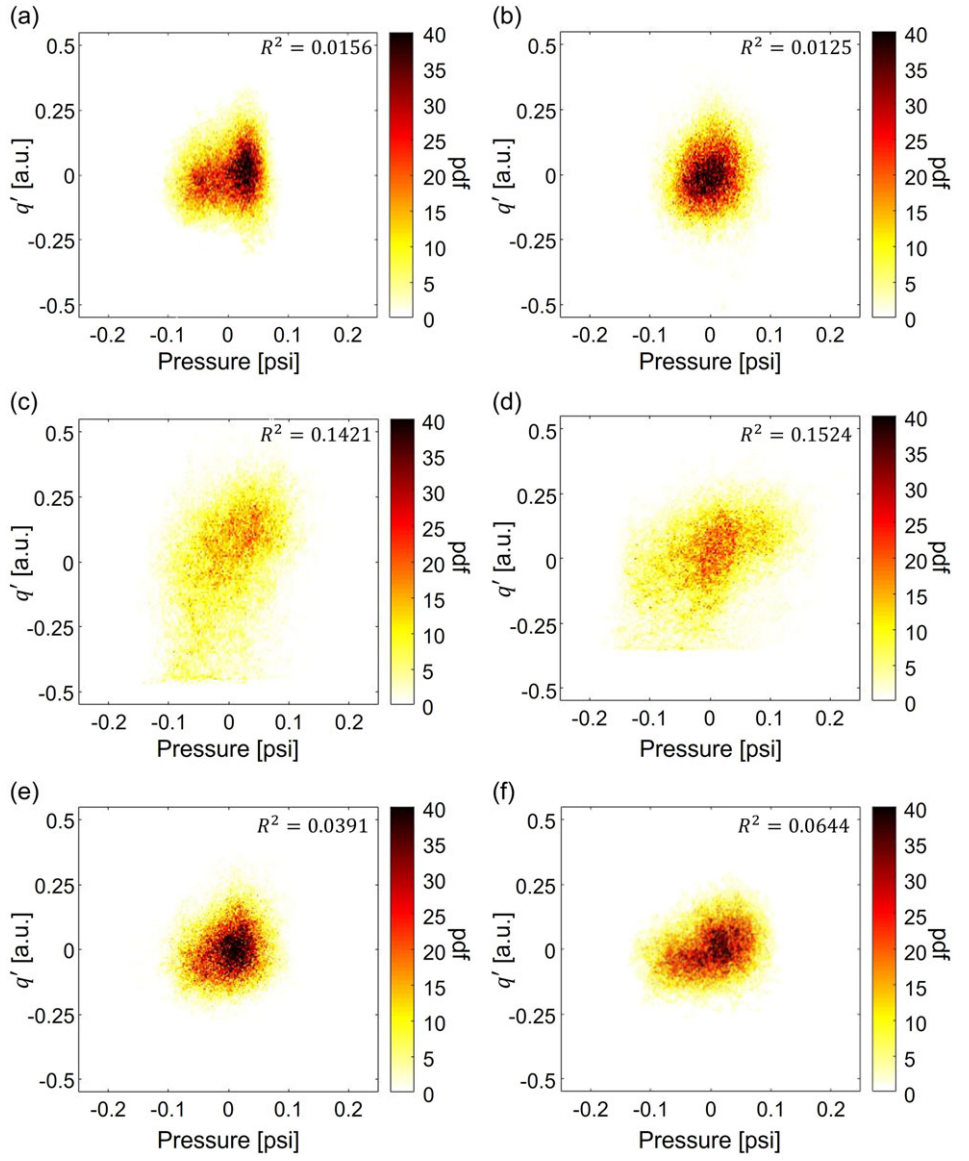

Figure 16. *Joint probability density distribution between p_3' and q' under $\phi_{af} = 0.58$ of (a) Jet-A, (b) A-2, (c) C-1, (d) C-5, (e) C-9, and (f) JP-8/HRJ flames.*

From the measurement of the shear layer reactivity of the test SAFs flame at the V-gutter, it is confirmed that the shear layer reactivity decreases as the ϕ_{af} approaches the LBO point, which implies that the strength of flame anchoring to the V-gutter becomes weakened. Conversely, the shear layer reactivity increases as the ϕ_{af} increases, which means that the flame is more strongly anchored to the V-gutter. However, above a certain ϕ_{af}, the shear layer reactivity decreases due to the flashback.

From the measurement of the pressure perturbation at the afterburner, the perturbation strength increases as the ϕ_{af} increases and it was confirmed that the perturbation is caused by thermo-acoustic combustion instability. For the flames by C-1 and C-5 with smaller DCN than other test fuels, the interaction between pressure and heat release rate perturbations is stronger than other test fuels, so the blowoff occurs at the high ϕ_{af} due to the strong combustion instability.

https://doi.org/10.1017/aer.2024.49 Published online by Cambridge University Press

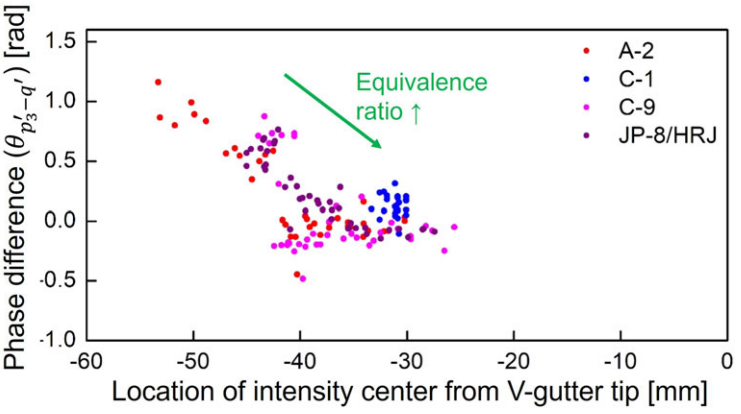

Figure 17. *Phase difference between p_3' and q' for each test fuel according to the location of intensity centre from V-gutter tip.*

In conclusion, the test fuels with a high DCN, a chemical property of the fuel, can be stabilised at lower equivalence ratios, show wider combustible ranges (including stable and flashback conditions) than test fuels with a small DCN, and have relatively small pressure perturbations, but have a higher risk of flashback. Conversely, the probability of the flashback is low for the test fuels with a small DCN, but they have narrower combustible ranges and higher-pressure perturbations. Therefore, these characteristics need to be considered when they are used in actual combustion engines.

This study explores the combustion characteristics such as LBO, flashback, and combustion instability of six SAFs in an in-tandem combustor and identifies the relationship between the fuel property and those combustion characteristics. Through this, the suitable fuel property and combustion conditions for stable combustion are identified. Therefore, the results will provide a reference for future studies on the SAFs including the NJFCP test fuels. Furthermore, this study demonstrated a unique experimental setup of an in-tandem combustor where two combustors interact each other. The future work will focus the interaction between the two combustors for a wider range of operating conditions, including the utilisation of SAF in the main combustor.

Acknowledgements. The authors would like to acknowledge the NRC Gas Turbine Laboratory team for setting up and performing this test, US AFRL for supplying the fuels and the Canadian Department of National Defence (DND) for their co-funding support.

References

[1] Colket, M., Heyne, J., Rumizen, M., Gupta, M., Edwards, T., Roquemore, W.M., Andac, G., Boehm, R., Lovett, J., Williams, R., Condevaux, J., Turner, D., Rizk, N., Tishkoff, J., Li, C., Moder, J., Friend, D. and Sankaran, V. Overview of the national jet fuels combustion program, *AIAA J.*, 2017, **55,** pp 1087–1104.

[2] Heyne, J.S., Peiffer, E., Colket, M.B., Jardines, A., Shaw, C., Moder, J.P., Roquemore, W.M., Edwards, J.T., Li, C. and Rumizen, M. Year 3 of the national jet fuels combustion program: practical and scientific impacts of alternative jet fuel research, 2018 AIAA Aerospace Sciences Meeting, 2018, p 1667.

[3] He, Z.J., Podboy, D. and Chang, C. Effects alternative fuels on gas emissions and combustion dynamic characteristics on a 9-point LDI combustor, 2018 AIAA Aerospace Sciences Meeting, 2018, p 2126.

[4] Corporan, E., Edwards, J.T., Stouffer, S., DeWitt, M., West, Z., Klingshirn, C. and Bruening, C. Impacts of fuel properties on combustor performance, operability and emissions characteristics, 55th AIAA Aerospace Sciences Meeting, 2017, p 0380.

[5] Allen, C., Valco, D., Toulson, E., Edwards, T. and Lee, T. Ignition behavior and surrogate modeling of JP-8 and of camelina and tallow hydrotreated renewable jet fuels at low temperatures, *Combust. Flame*, 2013, **160**, pp 232–239.

[6] Kang, D., Kim, D., Kalaskar, V., Violi, A. and Boehman, A.L., Experimental characterization of jet fuels under engine relevant conditions–Part 1: Effect of chemical composition on autoignition of conventional and alternative jet fuels, *Fuel*, 2019, **239,** pp 1388–1404.

[7] Zheng, L., Cronly, J., Ubogu, E., Ahmed, I., Zhang, Y. and Khandelwal, B. Experimental investigation on alternative fuel combustion performance using a gas turbine combustor, *Appl. Energy*, 2019, **238**, pp 1530–1542.

https://doi.org/10.1017/aer.2024.49 Published online by Cambridge University Press

[8] Casselberry, R.Q., Corporan, E. and DeWitt, M.J. Correlation of combustor lean blowout performance to supercritical pyrolysis products, *Fuel*, 2019, **252**, pp 504–511.
[9] Peiffer, E.E., Heyne, J.S. and Colket, M. Sustainable aviation fuels approval streamlining: Auxiliary power unit lean blowout testing, *AIAA J.*, 2019, **57**, pp 4854–4862.
[10] Alsulami, R., Lucas, S., Hageman, M., Knadler, M., Quinlan, J.M. and Windom, B. Coupling effects of physical and chemical properties on jet fuel spray flame blowout, *Proc. Combust. Inst.*, 2021, **38**, pp 3333–3341.
[11] Hosseinpour, S., Aghbashlo, M., Tabatabaei, M. and Khalife, E., Exact estimation of biodiesel cetane number (CN) from its fatty acid methyl esters (FAMEs) profile using partial least square (PLS) adapted by artificial neural network (ANN), *Energy Convers. Manag.*, 2016, **124**, pp 389–398.
[12] Westbrook, C.K., Pitz, W.J., Mehl, M. and Curran, H.J. Detailed chemical kinetic reaction mechanisms for primary reference fuels for diesel cetane number and spark-ignition octane number, *Proc. Combust. Inst.*, 2011, **33**, pp 185–192.
[13] Zheng, Z., Li, C., Liu, H., Zhang, Y., Zhong, X. and Yao, M. Experimental study on diesel conventional and low temperature combustion by fueling four isomers of butanol, *Fuel*, 2015, **141,** pp 109–119.
[14] Shanbhogue, S.J., Husain, S. and Lieuwen, T. Lean blowoff of bluff body stabilized flames: Scaling and dynamics, *Prog. Energy Combust. Sci.*, 2009, **35**, pp 98–120.
[15] Won, S.H., Rock, N., Lim, S.J., Nates, S., Carpenter, D., Emerson, B., Lieuwen, T., Edwards, T. and Dryer, F.L. Preferential vaporization impacts on lean blow-out of liquid fueled combustors, *Combust. Flame*, 2019, **205**, pp 295–304.
[16] Heyne, J.S., Colket, M.B., Gupta, M., Jardines, A., Moder, J.P., Edwards, J.T., Roquemore, M., Li, C. and Rumizen, M. Year 2 of the National jet fuels combustion program: Towards a streamlined alternative jet fuels certification process, 55th AIAA Aerospace Sciences Meeting, 2017, p 0145.
[17] Lovett, J., Brogan, T., Philippona, D., Kiel, B. and Thompson, T. Development needs for advanced afterburner designs, 40th AIAA/ASME/SAE/ASEE Joint Propulsion Conference and Exhibit, 2004, p 4192.
[18] Zukoski, E.E. Afterburners, 1978.
[19] Nakanishi, S., Velie, W.W. and Bryant, L. An investigation of effects of flame-holder gutter shape on afterburner performance, 1954.
[20] Chaudhuri, S., Kostka, S., Renfro, M.W. and Cetegen, B.M. Blowoff dynamics of bluff body stabilized turbulent premixed flames, *Combust. Flame*, 2010, **157**, pp 790–802.
[21] Jeong, C., Bae, J., Kim, T., Yoon, J., Joo, S. and Yoon, Y. Investigation of flashback characteristics coupled with combustion instability in turbulent premixed bluff body flames using high-speed OH-PLIF and PIV, *Proc. Combust. Inst.*, 2017, **36**, pp 1861–1868.
[22] Geikie, M.K. and Ahmed, K.A. Lagrangian mechanisms of flame extinction for lean turbulent premixed flames, *Fuel*, 2017, **194**, pp 239–256.
[23] Nair, S. and Lieuwen, T. Near-blowoff dynamics of a bluff-body stabilized flame, *J. Propul. Power*, 2007, **23**, pp 421–427.
[24] Tuttle, S.G., Chaudhuri, S., Kostka, S., Kopp-Vaughan, K.M., Jensen, T.R., Cetegen, B.M. and Renfro, M.W. Time-resolved blowoff transition measurements for two-dimensional bluff body-stabilized flames in vitiated flow, *Combust. Flame*, 2012, **159**, pp 291–305.
[25] Pathania, R.S., Skiba, A.W., Ciardiello, R. and Mastorakos, E., Blow-off mechanisms of turbulent premixed bluff-body stabilised flames operated with vapourised kerosene fuels, *Proc. Combust. Inst.*, 2021, **38**, pp 2957–2965.
[26] Leonard, P. and Mellor, A. Correlation of lean blowoff of gas turbine combustors using alternative fuels, *J. Energy*, 1983, **7**, pp 729–732.
[27] Plee, S. and Mellor, A. Characteristic time correlation for lean blowoff of bluff-body-stabilized flames, *Combust. Flame*, 1979, **35**, pp 61–80.
[28] Wang, Z., Hu, B., Zhao, Q. and Xu, J. Towards predicting lean blow-off based on Damköhler number and practical reaction zone, Turbo Expo: Power for Land, Sea, and Air, American Society of Mechanical Engineers, 2017, p V04AT04A039.
[29] Zhang, T., Hu, Z. and Zhou, Y. Numerical analysis on the characteristic chemical time scale and combustion regime of natural gas MILD combustion, *Fuel*, 2020, **282**, p 118811.
[30] Husain, S.A. *Analysis of Blowoff Scaling of Bluff Body Stabilized Flames*, Georgia Institute of Technology, 2008.
[31] Knaus, D., Magari, P., Hill, R., Phillips, S. and Kiel, B. Predicting augmentor static stability using local Damkohler number, 46th AIAA Aerospace Sciences Meeting and Exhibit, 2008, p 1027.
[32] Kalghatgi, G.T. Auto-ignition quality of practical fuels and implications for fuel requirements of future SI and HCCI engines, SAE Technical Paper 1, 2005, 0239.
[33] Gowdagiri, S., Wang, W. and Oehlschlaeger, M.A. A shock tube ignition delay study of conventional diesel fuel and hydroprocessed renewable diesel fuel from algal oil, *Fuel*, 2014, **128**, pp 21–29.
[34] Wang, H. and Oehlschlaeger, M.A. Autoignition studies of conventional and Fischer–Tropsch jet fuels, *Fuel*, 2012, **98**, pp 249–258.
[35] Vandersickel, A., Hartmann, M., Vogel, K., Wright, Y.M., Fikri, M., Starke, R., Schulz, C. and Boulouchos, K. The autoignition of practical fuels at HCCI conditions: High-pressure shock tube experiments and phenomenological modeling, *Fuel*, 2012, **93**, pp 492–501.
[36] Weisser, G.A. *Modelling of Combustion and Nitric Oxide Formation for Medium-Speed DI Diesel Engines: A Comparative Evaluation of Zero-and Three-Dimensional Approaches*, ETH Zurich, 2001.
[37] De Toni, A., Werler, M., Hartmann, R., Cancino, L., Schießl, R., Fikri, M., Schulz, C., Oliveira, A., Oliveira, E. and Rocha, M. Ignition delay times of Jet A-1 fuel: Measurements in a high-pressure shock tube and a rapid compression machine, *Proc. Combust. Inst.*, 2017, **36**, pp 3695–3703.

https://doi.org/10.1017/aer.2024.49 Published online by Cambridge University Press

[38] Wang, Z., Hu, B., Fang, A., Zhao, Q. and Chen, X. Analyzing lean blow-off limits of gas turbine combustors based on local and global Damköhler number of reaction zone, *Aerospace Sci. Technol.*, 2021, **111**, p 106532.
[39] Zhang, J., Chang, J., Ma, J., Wang, Y. and Bao, W. Investigations on flame liftoff characteristics in liquid-kerosene fueled supersonic combustor equipped with thin strut, *Aerospace Sci. Technol.*, 2019, **84**, pp 686–697.
[40] Carter, T.J. Common failures in gas turbine blades, *Eng. Failure Anal.*, 2005, **12**, pp 237–247.
[41] Paxton, B.T., Fugger, C.A., Tomlin, A.S. and Caswell, A.W. Experimental investigation of fuel chemistry on combustion instabilities in a premixed bluff-body combustor, AIAA Scitech 2020 Forum, 2020, p 0174.
[42] Marwan, N., Carmenromano, M., Thiel, M. and Kurths, J. Recurrence plots for the analysis of complex systems, *Phys. Rep.*, 2007, **438**, pp 237–329.
[43] Gotoda, H., Nikimoto, H., Miyano, T. and Tachibana, S. Dynamic properties of combustion instability in a lean premixed gas-turbine combustor, *Chaos*, 2011, **21**, p 013124.
[44] Edwards, J.T. Reference jet fuels for combustion testing, 55th AIAA Aerospace Sciences Meeting, 2017, p 0146.
[45] Yang, Z., Stachler, R. and Heyne, J.S. Orthogonal reference surrogate fuels for operability testing, *Energies*, 2020, **13**, p 1948.
[46] Won, S.H., Veloo, P.S., Dooley, S., Santner, J., Haas, F.M., Ju, Y. and Dryer, F.L. Predicting the global combustion behaviors of petroleum-derived and alternative jet fuels by simple fuel property measurements, *Fuel*, 2016, **168**, pp 34–46.
[47] Won, S.H., Haas, F.M., Dooley, S., Edwards, T. and Dryer, F.L. Reconstruction of chemical structure of real fuel by surrogate formulation based upon combustion property targets, *Combust. Flame*, 2017, **183**, pp 39–49.
[48] Standard test method for determination of ignition delay and derived cetane number (DCN) of diesel fuel oils by combustion in a constant volume chamber, American Society for Testing Materials: Designation: D 6890-03a, 2003.
[49] Chaudhuri, S., Kostka, S., Tuttle, S.G., Renfro, M.W. and Cetegen, B.M. Blowoff mechanism of two dimensional bluff-body stabilized turbulent premixed flames in a prototypical combustor, *Combust. Flame*, 2011, **158**, pp 1358–1371.
[50] Fan, A., Wan, J., Liu, Y., Pi, B., Yao, H. and Liu, W. Effect of bluff body shape on the blow-off limit of hydrogen/air flame in a planar micro-combustor, *Appl. Thermal Eng.*, 2014, **62**, pp 13–19.
[51] Hossain, A. and Nakamura, Y. A numerical study on the ability to predict the heat release rate using CH^* chemiluminescence in non-sooting counterflow diffusion flames, *Combust. Flame*, 2014, **161**, pp 162–172.
[52] Sardeshmukh, S., Bedard, M. and Anderson, W. The use of OH^* and CH^* as heat release markers in combustion dynamics, *Int. J. Spray Combust. Dyn.*, 2017, **9**, pp 409–423.
[53] Yan, S., Gong, Y., Guo, Q., Yu, G. and Wang, F. Numerical study of CH^* chemiluminescence and heat release rate in methane inverse diffusion flame, *Fuel*, 2024, **357**.
[54] Stouffer, S., Hendershott, T., Monfort, J.R., Diemer, J., Corporan, E., Wrzesinski, P. and Caswell, A.W. Lean blowout and ignition characteristics of conventional and surrogate fuels measured in a swirl stabilized combustor, 55th AIAA Aerospace Sciences Meeting, 2017, p 1954.
[55] Monfort, J.R., Stouffer, S., Hendershott, T., Wrzesinski, P., Foley, W. and Rein, K.D. Evaluating combustion instability in a swirl-stabilized combustor using simultaneous pressure, temperature, and chemiluminescense measurements at high repetition rates, 55th AIAA Aerospace Sciences Meeting, 2017, p 1101.
[56] Lieuwen, T.C. Investigation of combustion instability mechanisms in premixed gas turbines, Georgia Institute of Technology, 1999.
[57] Bae, J., Jeong, S. and Yoon, Y., Effect of delay time on the combustion instability in a single-element combustor, *Acta Astronaut.*, 2021, **178**, pp 783–792.

Cite this article: Bae J., Chaudhuri S., Canteenwalla P. and Yun S. (2024). Combustion characteristics of sustainable aviation fuels in a scaled-down afterburner test rig. *The Aeronautical Journal*, **128**, 1429–1449. https://doi.org/10.1017/aer.2024.49